Local atomic and electronic structure of $Al_{90}Fe_xCe_{10-x}$ alloys: XAFS analysis

A. N. Mansour,[a*] G. Cibin,[b] A. Marcelli,[b] T. Sevastyanova,[c] G. Yalovega,[c] and A. V. Soldatov[c]

[a]Naval Surface Warfare Center, Carderock Division, West Bethesda, MD 20817-5700, USA, [b]LNF, INFN Frscati, Italy, [c]Faculty of Physics, Rostov State University, 5 Sorge, Rostov-na-Donu, 344090, Russia.
Email: MansourAN@nswccd.navy.mil

X-ray absorption fine structure (XAFS) above the Fe K-edge and the Ce L_3-edge in amorphous $Al_{90}Fe_xCe_{10-x}$ (x = 3, 5, and 7) alloys have been measured and analyzed. Quantitative analyses of the Fe K-edge and Ce L_3-edge EXAFS spectra are limited to local structure parameters of the first coordination sphere. Using a theoretical multiple scattering (MS) approach, we show that the Fe and Ce XANES are sensitive to the structure of coordination spheres, which extend up to nearly 4.5 Å. Comparison of experimental XANES spectra with theoretical MS results allows one to determine the local structure around the iron and cerium sites up to at least the third shell of atoms.

Keywords: Aluminium-based alloys, Al-Fe-Ce, amorphous metals, X-ray absorption spectroscopy, XANES, EXAFS.

1. Introduction

Liquid-quenched amorphous $Al_{90}Fe_xCe_{10-x}$ (x = 3, 5, and 7) alloys combine the properties of a metal with the short-range order of a glass (Hseih et al., 1990 & 1991). Their structural characteristics led to a number of remarkable mechanical (Shiflet et al., 1988), magnetic (Wagner et al., 1989), and corrosion (Mansour & Melendres, 1995; Mansour et al., 1996) properties. These alloys have high strength, high ductility, low density, and high resistance to corrosion. Determination of the atomic and electronic structure of these alloys is essential in order to understand the origin of these properties. Therefore, the structure of these alloys was investigated by pulsed neutron and x-ray scattering methods (Hseih et al., 1990, 1991). The structure of vapor-quenched amorphous $Al_{100-2x}Co_xCe_x$ (x = 8, 9, and 10) and $Al_{80}Fe_{10}Ce_{10}$ was investigated by x-ray absorption fine structure (XAFS) analysis (Mansour et al., 1994).

In this investigation, the Fe K-edge and the Ce L_3-edge XAFS of amorphous $Al_{90}Fe_xCe_{10-x}$ (x = 3, 5, and 7) alloys have been measured and analyzed. The goal is to determine the best model for the local structure of the $Al_{90}Fe_xCe_{10-x}$ system and to study the peculiarities of the electronic structure of these alloys using XAFS analysis. Fourier transforms of the Fe K-edge and Ce L_3-edge EXAFS spectra (not shown here) display prominent contributions from the first coordination spheres of Fe and Ce, respectively, with no significant contributions from higher coordination spheres due to the amorphous nature of these alloys. Hence, quantitative analyses of EXAFS spectra are limited to the first coordination spheres of Fe and Ce (Table 1). The local structure parameters for Fe are independent of the composition range investigated here. Fe is coordinated with approximately 6.6 Al atoms at a distance of 2.46 Å. The disorder for the Fe-Al sphere is within the range expected for crystalline materials such as those for metallic Cu and Fe (Sevillano et al., 1979). The Ce-Al coordination sphere, on the other hand, consists approximately of 14 Al atoms at a distance which increased from 3.13 Å to 3.18Å in going from x = 7 to 3. The Ce-Al coordination is characterized by a high degree of structural disorder suggesting a distribution of Ce-Al distances in close proximity of each other. For comparison purposes, we have also included the structure parameters for crystalline $Al_{90}Fe_3Ce_7$. Clearly, the Fe-Al distance increased from 2.46 to 2.56 Å in going from a-$Al_{90}Fe_3Ce_7$ to c-$Al_{90}Fe_3Ce_7$ without a significant change in the Fe-Al coordination and disorder. The Ce-Al distance increased from 3.18 to 3.25 Å in going from a-$Al_{90}Fe_3Ce_7$ to c-$Al_{90}Fe_3Ce_7$ without a significant change in coordination. However, the Ce-Al disorder decreased from 0.0206 to 0.0081 $Å^2$ in going from a-$Al_{90}Fe_3Ce_7$ to c-$Al_{90}Fe_3Ce_7$ indicating a higher degree of structural disorder for the Ce-Al relative to that of the Fe-Al environment in the amorphous state.

Table 1
Structure parameters for Fe and Ce as determined from analysis of the Fe K-edge and the Ce L_3-edge EXAFS spectra for amorphous (a) and crystalline (c) alloys. N, R, and σ^2 are the coordination number, distance, and mean square relative displacement, respectively. N and σ^2 are accurate to ± 10% and R to ± 0.02 Å. The c-$Al_{90}Fe_3Ce_7$ alloy was obtained by heating the a-$Al_{90}Fe_3Ce_7$ alloy.

Sample	X-Y Pair	N	R (Å)	$\sigma^2(10^{-3}Å^2)$
a-$Al_{90}Fe_7Ce_3$	Fe-AL	6.6	2.46	7.7
	Ce-Al	14.0	3.13	18.5
a-$Al_{90}Fe_5Ce_5$	Fe-AL	6.6	2.46	7.5
	Ce-Al	13.4	3.15	18.7
a-$Al_{90}Fe_3Ce_7$	Fe-AL	6.7	2.46	7.7
	Ce-Al	13.9	3.18	20.6
c-$Al_{90}Fe_3Ce_7$	Fe-AL	7.7	2.56	8.4
	Ce-Al	12.3	3.25	8.1

Hence, the goal is to explore the XANES region and determine if extra structural information with regard to higher coordination spheres can be obtained on the basis of multiple scattering (MS) analysis. The MS approach used in this investigation has been successfully applied in order to interpret a large number of XANES for various materials (Durham, 1989; Fujikawa et al., 1983; Vvedensky et al., 1986; Della Longa et al., 1995; Vedrinskii et al., 1998; Rehr & Albers, 2000). The analysis has been found rather powerful for the case of ordered alloys like Ni_3Al and $NiAl_3$ (Mansour et al., 1997) but no such analysis has been applied to the study of amorphous $Al_{90}Fe_xCe_{10-x}$ alloys. We show that analysis of XANES data enabled us to choose the best structural model including symmetry for the alloys investigated.

2. Experiment and Method of Calculation

Amorphous samples in the form of 25 μm thick ribbons with nominal compositions $Al_{90}Fe_xCe_{10-x}$ (x = 3, 5, and 7) were prepared by rapid solidification from the liquid phase (He et al., 1988). The room temperature Fe K-edge and Ce L_3-edge XAFS spectra were measured in transmission mode on beamline X-11A at the National Synchrotron Light Source. Details of experimental setup were published elsewhere (Mansour et al. 1996). The energy resolution in the measured interval is about 1.0 eV. The Fe K-edge and Ce L_3-edge XANES for the amorphous alloys are essentially the same in the composition range investigated here.

The algorithm of the scattering wave method was described earlier (Della Longa et al., 1995). The local structure around the iron and cerium sites of $Al_{90}Fe_xCe_{10-x}$ alloy was treated using structural models based on crystalline $FeAl_6$ and $CeAl_4$ (Villars & Calvert, 1985) and $FeAl_3$ (Black, 1955). The structure parameters for the Fe clusters used in the calculations are reported in Table 2 (crystalline $FeAl_3$) and in Table 3 (crystalline $FeAl_6$). Fe in $FeAl_3$ is present in five non-equivalent sites (see Table 2). In this case, the theoretical spectrum represents the weighted average of contributions from all non-equivalent sites. The theoretical spectrum for $FeAl_6$ was also calculated using actual atomic distances reduced by 3.4%. The reduced atomic distances provide

a better agreement with the experimental XANES data. Two clusters around Ce were used: one model using the structure data for crystalline $CeAl_4$ (Table 4) and the other was obtained using atomic distances for crystalline $CeAl_4$ reduced by 6% (Table 4).

Table 2
Structure parameters for crystalline $FeAl_3$. Fe in $FeAl_3$ has five non-equivalent sites with multiplicity of 4, 4, 4, 4, and 8 for sites 1, 2, 3, 4, and 5, respectively.

Shell number (site)	X-Y Pair	N	R (Å)
1 (1)	Fe-Al	4	2.324
2 (1)	Fe-Al	4	2.630
3 (1)	Fe-Al	3	2.803
1 (2)	Fe-Al	6	2.532
2 (2)	Fe-Al	4	2.737
3 (2)	Fe-Al/Fe	6	4.180
1 (3)	Fe-Al	4	2.353
2 (3)	Fe-Al	4	2.559
3 (3)	Fe-Al/Fe	3	2.823
1 (4)	Fe-Al	8	2.518
2 (4)	Fe-Al	2	2.752
3 (4)	Fe-Fe	1	3.005
1 (5)	Fe-Al	3	2.389
2 (5)	Fe-Al	5	2.578
3 (5)	Fe-Al	3	3.328

Table 3
Structure parameters for crystalline $FeAl_6$. Distances in parentheses correspond to actual distances reduced by 3.4%.

Shell number	X-Y Pair	N	R (Å)
1	Fe-Al	10	2.547(2.460)
2	Fe-Al/Fe	10	4.204(4.061)
3	Fe-Al	6	4.537(4.375)

Table 4
Structure parameters for crystalline $CeAl_4$. Distances in parentheses correspond to actual distances reduced by 6%.

Shell number	X-Y Pair	N	R (Å)
1	Ce-Al	16	3.341(3.141)
2	Ce-Al	2	3.805(3.577)
3	Ce-Ce	4	4.374(4.112)

Phase shifts were calculated in the framework of the crystal muffin-tin (MT) potential scheme with touching MT spheres. The MT radii and the MT constants were obtained according to an established procedure of MT potential construction (Della Longa et al., 1995). The MT approximation according to the Mattheiss prescription with exchange parameter equal to 1.0 was used while constructing the crystal potential. Atomic charge densities were obtained with the help of a self-consistent Dirac-Slater method.

It is well known (Muller et al., 1982) that within the dipole approximation the x-ray absorption coefficient, $\alpha(E)$, for the Fe K-edge is given by

$$\alpha(E) \sim |m_L(E)|^2 N_p^{Fe}(E) \qquad (1)$$

where $N_p^{Fe}(E)$ is the partial density of unoccupied Fe states with *p*-symmetry and $m_L(E)$ is the normalized dipole transition matrix element given by

$$m_L(E) = \frac{\int dr\ \Phi_l(r,E)\ \Delta(r)\ \Psi_c(r)}{[\int dr\ \Phi^2{}_l(r,E)]^{1/2}} \qquad (2)$$

where $\Phi_l(r,E)$ is a solution of the radial Schrodinger equation at energy E for MT potential (l = 1 for the K-edge), $\Delta(r)$ is the electron-photon interaction operator, and $\Psi c\ (r)$ is the core *K*-level wave function. In the calculation, phase shifts with orbital momentum (l) up to 4 have been included even though there is almost no change in the spectra when compared with those calculated with l up to 2. For the Ce L_3-edge XANES, the situation in general is more complicated. There are two dipole channels (p->d and p->s), so the Ce XANES corresponds to the density of unoccupied states with s- and d-symmetry. However, the transition matrix element for the p->s is about 50 times smaller than that for the p->d transition. Hence, it is sufficient to take into account only the contribution of the p->d transition.

3. Results and Discussion

In order to perform a direct comparison with experimental data one must take into account two factors. One factor is the filling of the occupied states following the Fermi distribution. The other factor is the broadening of experimental spectra due to the core hole lifetime, the finite mean free path of the photoelectron, and the experimental resolution. For the bandwidth of the core hole, a 1.25 eV for the Fe XANES and a 3.48 eV for the Ce XANES were used (Fuggle & Inglesfield, 1992). The energy dependent function obtained by Muller et al. (1982) was used for the mean free path of the photoelectron. For the experimental energy resolution a value of 1.0 eV was used. These factors were treated as contributions to the imaginary part of the self-energy term.

In addition, one must compare the experimental data with the theoretical calculation made using a relaxed potential (i.e., taking into account the presence of the core hole). This effect was treated in the Z+1 approximation (Mansour et al., 1997) and found that for the K-edge the contribution of the core hole is rather small, while for the Ce L_3 edge, the core hole effect is more important (Soldatov et al., 1993). Since Ce is not in the tetravalent state in the alloys under study (Mansour et al., 1996), one does not need to take into account many-body effects like in the case of tetravalent Ce in CeO_2 (Soldatov et al., 1994).

In Fig.1, we present a comparison of theoretical XANES spectra calculated using the structure data for the $FeAl_6$ alloy as a function of cluster size. The calculations were made using atomic distances reduced by 3.4% from the actual distances. Clearly, the XANES features are dominated by the contribution from the first shell of atoms (cluster size of 2.46 Å). However, expanding the cluster size to include the second and third shells of atoms is essential in order to reproduce all of the features observed in the experimental Fe XANES for the amorphous alloys. In Fig. 2, we present comparison of experimental Fe K-edge XANES for amorphous $Al_{90}Fe_3Ce_7$ and theoretical Fe K-edge XANES calculated for two model alloys "$FeAl_3$" and "$FeAl_6$" (Tables 2 and 3). The theoretical XANES for both models are qualitatively similar. However, according to the energy position of peak C as well as the double A-A' structure, the "$FeAl_6$" model with atomic distances reduced by 3.4% gives a better agreement with the experimental data. Hence, we conclude that the local structure around the Fe site in a-$Al_{90}Fe_3Ce_7$ is closer to the one deduced from crystalline $FeAl_6$ with atomic distances reduced by 3.4%. It is to be noted that the Fe-Al distance in a-$Al_{90}Fe_3Ce_7$ is reduced by 3.9% from that in c-$Al_{90}Fe_3Ce_7$ (Table 1).

Comparison of experimental Ce L_3-edge XANES of a-$Al_{90}Fe_3Ce_7$ and theoretical XANES spectra calculated using actual atomic distances for crystalline $CeAl_4$ (model 1, Table 4) and those reduced by 6% (model 2, Table 4) are presented in Fig. 3. Clearly, the theoretical spectrum of model 2 is in better agreement with the experimental spectrum of a-$Al_{90}Fe_3Ce_7$. Thus, we conclude that the local structure of the Ce site in the amorphous alloys is better described by the structure parameters of crystalline $CeAl_4$ with atomic distances reduced by 6%.

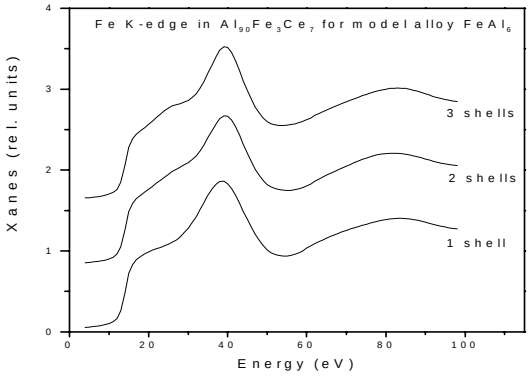

Figure 1
Theoretical XANES spectra calculated as a function of cluster size using structure data for crystalline $FeAl_6$ with atomic distances reduced by 3.4% from the actual distances (Table 3).

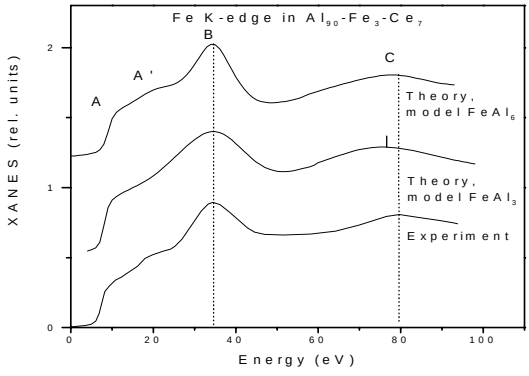

Figure 2
Experimental Fe K-edge XANES for a-$Al_{90}Fe_3Ce_7$ compared with theoretical XANES for crystalline $FeAl_3$ (Table 2) and $FeAl_6$ (Table 3). The XANES for $FeAl_6$ was calculated with distances reduced by 3.4%.

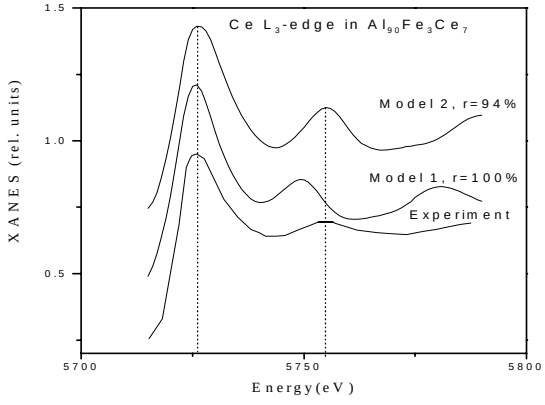

Figure 3
Experimental Ce L_3-edge XANES for a-$Al_{90}Fe_3Ce_7$ compared with theoretical XANES calculated for crystalline $CeAl_4$ using actual distances (model 1) and those reduced by 6% (model 2). See Table 4 for details.

Another factor (beyond phase shifts and cluster local structure) that determines the XANES is the transition matrix element (2) that influences the relative intensity of the XANES features. Since the energy dependence of the dipole transition matrix element is non-oscillatory in nature in the region above 30 eV from the absorption threshold, one can use the Fe K-edge XANES of these alloys to study the density of unoccupied Fe states with *p*-symmetry in the conduction band.

4. Conclusions

Theoretical analysis of experimental XAFS on the basis of multiple scattering theory has been applied to study the peculiarities of the local atomic and electronic structure of amorphous $Al_{90}Fe_xCe_{10-x}$ alloys. Comparison of experimental and theoretical XANES above the Fe K-edge and the Ce L_3edge enabled us to determine the local structure around the Fe and Ce sites up to the third shell. Results from analysis of EXAFS spectra were limited to local structure parameters of the first shell. It is to be noted that the fine structure of the Fe *p*- density of unoccupied states in the low energy region evolves from a large cluster, which includes at least three shells

We are thankful to Prof. S. J. Poon of the University of Virginia for providing the samples. ANM acknowledges financial support by the ILIR Program of NSWCCD. Beamline X-11A and NSLS are supported by the USDOE under Contract Nos. DE-AS05-80-ER-10742 and DE-AC02-76CH00016, respectively.

References

Black P. J. (1955). Acta Cryst. **8**, 43-48 &175-182.
Durham, P. J. (1988). X-ray Absorption: Principles, Applications, Techniques of EXAFS, SEXAFS, and XANES, edited by D. C. Koningsberger & R. Prins, pp. 53-84. New York: John Wiley & Sons.
Della Longa, S., Soldatov, A. V., Pompa, M. & Bianconi, A. (1995). Computational Materials Science **4**, 199-210.
Fuggle, J. C. & Inglesfield, J. E. Editors (1992). Unoccupied Electronic States. Berlin: Springer.
Fujikawa, T., Matsuura, T. & Kuroda H. (1983). J. Phys. Soc. Jpn **52(3)**, 905-912.
He, Y., Poon, S. J. & Shiflet, G. J. (1988). Science **241(9)**, 1640-1642.
Hseih, H. Y., Toby, B. H., Egami, T., He, Y. & Poon, S. J. (1990). J. Mater. Res. **5(12),** 2807-2812.
Hseih, H.Y., Egami, T., He, Y, Poon, S. J, & Shiflet, G.F. (1991). J. Non-Cryst. Solids **135**, 248-254.
Mansour, A. N., Dmitrienko A. & Soldatov, A. V. (1997). Phys. Rev**.** B**55(23),** 15531-15536.
Mansour, A. N. & Meledres, C. A. (1995). J. Electrochem. Soc. **142(6)**, 1961-1967.
Mansour, A. N., Meledres, C. A., Poon, S. J, He, Y., & Shiflet, G. J. (1996). J. Electrochem. Soc. **143(2)**, 614-619.
Mansour, A. N., Wong, C.-P., &. Brizzolara, R. A. (1994). Phys. Rev. B**50(17)**, 12401-12411.
Muller, J. E., Jepsen, O. & Wilkins, J. W. (1982). Solid State Commun. **42(5)**, 365-368.
Rehr, J. J. & Albers, R. C. (2000). Rev. Mod. Phys. **72(3)**, 621-654.
Sevillano, E., Meuth, H. & Rehr, J. J. (1979). Phys. Rev. B**20(12)**, 4908-4911.
Shiflet, G. J., He, Y. & Poon, S. J. (1988). J. Appl. Phys. **64(12)**, 6863-6865.
Soldatov, A. V., Della Longa, S. & Bianconi, A. (1993). Solid State Commun. **85(10)**, 863-868.
Soldatov, A. V., Ivanchenko, T. S., Della Longa, S, Kotani, A., Iwamoto, Y. & Bianconi, A. (1994). Phys. Rev**.** B**50(8),** 5074-5080.
Vedrinskii, R. V., Kraizman, V. L., Novakovich, A. A. Demekhin, Ph. V. & Urazhdin, S. V. (1998). J. Phys.: Condens. Matter **10(42)**, 9561-9580.
Vvedensky D. D., Saldin, D. K. & Pendry J. B. (1986). Comput. Phys. Commun. **40**, 421-440.
Villars, P. & Calvert, L. D. (1985). Pearson's Handbook of Crystallographic Data for Intermetallic Phases, vol. 2, pp. 920-920 & 972-973, American Society for Metals, Metals Park, OH.
Wagner, J. L., Wong, K. M., Pierce, F. S. & Poon, S. J. (1989). Phys. Rev. B**39(8),** 5500-5503.

 Received 31 July 2000 • Accepted 10 November 2000